Inorganic Chemistry

Article

pubs.acs.org/IC

Water Oxidation with Mononuclear Ruthenium(II) Polypyridine Complexes Involving a Direct Ru^{IV}=O Pathway in Neutral and Alkaline Media

Yosra M. Badiei,[†] Dmitry E. Polyansky,*[,†] James T. Muckerman,[†] David J. Szalda,[‡] Rubabe Haberdar,[§] Ruifa Zong,[§] Randolph P. Thummel,[§] and Etsuko Fujita*[,†]

[†]Chemistry Department, Brookhaven National Laboratory, Upton, New York 11973-5000, United States

[‡]Department of Natural Science, Baruch College, CUNY, New York, New York 10010, United States

[§]Department of Chemistry, University of Houston, Houston, Texas 77204-5003, United States

Supporting Information

ABSTRACT: The catalytic water oxidation mechanism proposed for many single-site ruthenium complexes proceeds via the nucleophilic attack of a water molecule on the Ru^{V}=O species. In contrast, Ru(II) complexes containing 4-*t*-butyl-2,6-di-1′,8′-(naphthyrid-2′-yl)-pyridine (and its bisbenzo-derivative), an equatorial water, and two axial 4-picolines follow the thermodynamically more favorable "direct pathway" via $[Ru^{IV}=O]^{2+}$, which avoids the higher oxidation state $[Ru^{V}=O]^{3+}$ in neutral and basic media. Our experimental and theoretical results that focus on the pH-dependent onset catalytic potentials indicative of a PCET driven low-energy pathway for the formation of products with an O−O bond (such as $[\mathbf{Ru^{III}}-OOH]^{2+}$ and $[\mathbf{Ru^{IV}}-OO]^{2+}$) at an applied potential below the Ru^{V}=O/Ru^{IV}=O couple clearly support such a mechanism. However, in the cases of $[Ru(tpy)(bpy)(OH_2)]^{2+}$ and $[Ru(tpy)(bpm)(OH_2)]^{2+}$, the formation of the Ru^{V}=O species appears to be required before O−O bond formation. The complexes under discussion provide a unique functional model for water oxidation that proceeds by four consecutive PCET steps in neutral and alkaline media.

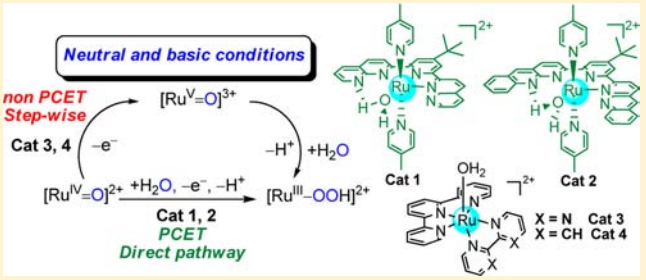

INTRODUCTION

Water oxidation ($2H_2O \rightarrow 4H^+ + 4e^- + O_2$) is an energetically demanding and critical half reaction for the development of clean and sustainable fuel technologies.[1−8] The photosynthetic oxygen-evolving complex (OEC) in photosystem II can oxidize water to oxygen at a potential near the thermodynamic limit (1.23 V vs NHE at pH 0) by taking advantage of energetically favorable proton-coupled electron transfer (PCET) pathways.[9−13] Thus, it is important to develop new water-oxidation catalysts (WOC) that can efficiently mediate the four consecutive PCET steps and thereby minimize undesirable overpotentials.[14] Molecular catalysts with low overpotentials are also crucial for developing photochemical (light-driven) water oxidation since typical photosensitizers such as $[Ru(bpy)_3]^{2+}$ (1.26 V vs NHE) have lower redox potentials than the ubiquitous sacrificial oxidant Ce(IV). Note that all potentials are reported vs NHE in this paper.

Following the discovery in 1982 by Meyer and co-workers of the molecular WOC[15] known as the "blue dimer," in 2005 Zong and Thummel reported on a mononuclear Ru(II) polypyridine WOC.[16] This discovery spurred interest in developing a number of mononuclear ruthenium WOCs both in the homogeneous phase[8,17−33] and more recently immobilized on heterogeneous surfaces.[4,6,34−40] Furthermore, Sun and Llobet have reported a number of Ru(II) bipyridine−dicarboxylate complexes with high turnover frequencies (TOFs) comparable to the reaction rate of photosystem II.[29,41]

In general, O_2 evolution catalyzed by these complexes in Ce(IV)-driven water oxidation (acidic pH) proceeds by the nucleophilic attack of a water molecule[18,42−44] on a high-valent $[Ru^{V}=O]^{2+}$ species formed by a non-PCET electron transfer step from $[Ru^{IV}=O]^{2+}$ at high overpotential (>400 mV) to produce a hydroperoxo intermediate $[Ru^{III}-OOH]^{2+}$ in the water oxidation mechanism.[18,20−22,42] However, another water oxidation mechanism has been proposed proceeding via O−O bond formation through the interaction of two mononuclear M=O units.[29,41]

Using various spectroscopic, electrochemical, and mass spectrometric labeling techniques in conjunction with density functional theory (DFT) calculations, we have recently elucidated the mechanism of water oxidation catalyzed by $[\mathbf{Ru^{II}(1)}-OH_2]^{2+}$ ($\mathbf{Ru^{II}(1)}$ = ruthenium(II) coordinated with 4-*t*-butyl-2,6-di-1′,8′-(naphthyrid-2′-yl)-pyridine (NPM) and two 4-picoline ligands),[23] and have provided a detailed characterization of the catalytic intermediates such as

Received: April 27, 2013
Published: July 9, 2013

dx.doi.org/10.1021/ic401023w | *Inorg. Chem.* 2013, 52, 8845−8850

$[\mathbf{Ru^{III}(1)}-OH]^{2+}$, $[\mathbf{Ru^{IV}(1)}=O]^{2+}$, and $[\mathbf{Ru^{IV}(1)}-OO]^{2+}$. Intriguingly, the $[\mathbf{Ru^{IV}(1)}=O]^{2+}$ species, which is formed from $[\mathbf{Ru^{II}(1)}-OH_2]^{2+}$ by an initial coupled two-electron, two-proton step, can react directly with a water molecule to generate $[\mathbf{Ru^{III}(1)}-OOH]^{2+}$ and then $[\mathbf{Ru^{IV}(1)}-OO]^{2+}$ in two successive PCET events at pH > 3. While the formation of $[\mathbf{Ru^{III}(1)}-OOH]^{2+}$ can proceed via formation of $[\mathbf{Ru^{V}(1)}=O]^{3+}$ followed by nucleophilic attack by a water molecule in an acidic solution, the reaction of $[\mathbf{Ru^{IV}}=O]^{2+}$ with a water molecule accompanied by the concomitant removal of an electron and a proton ("direct pathway") becomes predominant at higher pH.[23]

Herein we show that the O−O bond formation in water oxidation for the family of compounds of $[\mathbf{Ru^{II}(1)}-OH_2]^{2+}$ and $[\mathbf{Ru^{II}(2)}-OH_2]^{2+}$, ($\mathbf{Ru^{II}(2)}$ = ruthenium(II) coordinated with 2,6-bis(benzo[*b*]-1′,8′-naphthyridin-2′-yl)-4-*t*-butylpyridine, BNPM, and two 4-picoline ligands) (Chart 1) proceeds via the "direct pathway" described above under neutral and high pH conditions. By contrast, other Ru(II) polypyridyl complexes such as $[Ru(tpy)(bpy)(OH_2)]^{2+}$ (tpy = 2,2′;6′,2″-terpyridine, bpy = 2,2′-bipyridine) and $[Ru(tpy)(bpm)(OH_2)]^{2+}$ (bpm = 2,2′-bipyrimidine) studied under the same conditions appear strictly to follow the "non-PCET pathway" that forms the key catalytic intermediate $[Ru^{V}=O]^{3+}$ even in basic media.

Chart 1. Molecular Structures of Complexes $[\mathbf{Ru^{II}(1)}-OH_2]^{2+}$ and $[\mathbf{Ru^{II}(2)}-OH_2]^{2+}$

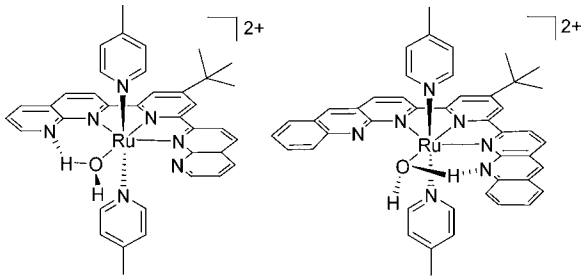

$[\mathbf{Ru^{II}(1)}-OH_2]^{2+}$ $[\mathbf{Ru^{II}(2)}-OH_2]^{2+}$

RESULTS AND DISCUSSION

Structure of $[\mathbf{Ru^{II}(2)}-OH_2]^{2+}$. The mononuclear $[\mathbf{Ru^{II}(2)}-OH_2]^{2+}$ complex was prepared as a synthetic analogue of $[\mathbf{Ru^{II}(1)}-OH_2]^{2+}$ by introducing two benzo groups to the 1,8-dinaphthyridyl ligand moieties (details are provided in the Supporting Information). The single-crystal X-ray structure of the $[\mathbf{Ru^{II}(2)}-OH_2]^{2+}$ complex shows that the bond distances and angles around the ruthenium center are similar to those[16] of $[\mathbf{Ru^{II}(1)}-OH_2]^{2+}$ (Figure 1; see Supporting Information, Tables S2 and S3). Interestingly the X-ray structure of $[\mathbf{Ru^{II}(2)}-OH_2]^{2+}$ indicates that the benzo-1,8-naphthyridine rings are stacked with a symmetry related molecule with a distance of 3.35 Å between the best planes of the aromatic rings in the two molecules as shown in Supporting Information, Figure S1. No such stacking is observed in $[\mathbf{Ru^{II}(1)}-OH_2]^{2+}$. In $[\mathbf{Ru^{II}(1)}-OH_2]^{2+}$ the O···N-(naphthyridine) distances are asymmetric with distances of 2.708(8) and 2.891(8) Å with the "longer" distance reported to be involved in the hydrogen bonding, whereas in the case of $[\mathbf{Ru^{II}(2)}-OH_2]^{2+}$ the O···N(naphthyridine) distances are equidistant at 2.749(5) Å. Although we could not locate the intramolecular hydrogen bonding interaction with certainty in

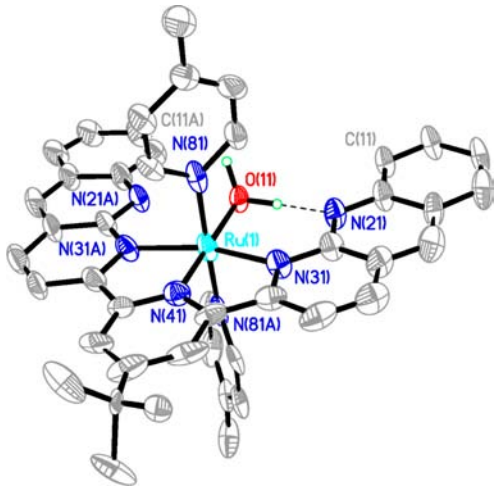

Figure 1. View of X-ray structure of $[\mathbf{Ru^{II}(2)}-OH_2]^{2+}$ with thermal ellipsoids at 25%.

$[\mathbf{Ru^{II}(2)}-OH_2]^{2+}$, our proposed model suggests that two hydrogen bonds may be involved: one between the coordinated water O(1) and the noncoordinated naphthyridine nitrogen, and another between the coordinated water O(1) and F(12) of the PF_6 anion (Figures 1 and Supporting Information, Figure S2). In solution, $[\mathbf{Ru^{II}(2)}-OH_2]^{2+}$ exhibits a relatively high pK_a (>12.5) (Supporting Information, Figure S3) similar to $[\mathbf{Ru^{II}(1)}-OH_2]^{2+}$ (>13.5)[23] which is consistent with their solid-state structures and supports the engagement of the water molecule in H-bonding. Our calculated structure of $[\mathbf{Ru^{II}(2)}-OH_2]^{2+}$ with one explicit molecule of water solvent shows unequal O···N(naphthyridine) distances, with the shorter one being associated with a hydrogen bond to the coordinated water molecule. The other hydrogen atom of the coordinated water molecule is hydrogen bonded to the explicit solvent molecule (Supporting Information, Figure S4).

Comparison of Chemical Properties and Water-Oxidation Catalytic Activities of $[\mathbf{Ru^{II}(2)}-OH_2]^{2+}$ and $[\mathbf{Ru^{II}(1)}-OH_2]^{2+}$. The downfield region of the ^{1}H NMR spectrum of $[\mathbf{Ru^{II}(2)}-OH_2]^{2+}$ is shown in Supporting Information, Figure S5. Spectroscopic and redox properties of $[\mathbf{Ru^{II}(2)}-NCMe]^{2+}$ and $[\mathbf{Ru^{II}(1)}-NCMe]^{2+}$ in acetonitrile are summarized in Supporting Information, Table S5. Note that the aqua complexes can readily change to the corresponding acetonitrile adducts. Moreover, the O_2-evolving ability of $[\mathbf{Ru^{II}(2)}-OH_2]^{2+}$ was evaluated and compared to that of $[\mathbf{Ru^{II}(1)}-OH_2]^{2+}$, which revealed similar catalytic performance in Ce(IV)-driven water-oxidation (pH 1.0). O_2 was evolved in significant amounts from solutions containing [Ru] = 2.0×10^{-5} M and [Ce^{IV}] = 4.5×10^{-2} M (Supporting Information, Figure S6) using procedures for the oxygen measurement and turnover number (TON) determination described in the Supporting Information. As shown in Figure 2, the initial rates of O_2 evolution were found to be first order in both $[Ru^{II}-OH_2]^{2+}$ and Ce(IV) concentrations (pH 1, 0.1 M HNO_3). The turnover frequencies (TOFs) for $[\mathbf{Ru^{II}(1)}-OH_2]^{2+}$ and $[\mathbf{Ru^{II}(2)}-OH_2]^{2+}$ that were determined from the pseudo first-order rate constants, k_{obs}, were larger than that of $[Ru(tpy)(bpm)(OH_2)]^{2+}$ by approximately an order of magnitude under similar catalyst concentrations with 0.01 M Ce(IV) (left panel of Figure 2). The second-order rate constants for O_2 evolution by $[\mathbf{Ru^{II}(1)}-OH_2]^{2+}$ and $[\mathbf{Ru^{II}(2)}-OH_2]^{2+}$ are comparable: k_{O2} = 2.2 ± 0.1 M^{-1} s^{-1}

dx.doi.org/10.1021/ic401023w | Inorg. Chem. 2013, 52, 8845−8850

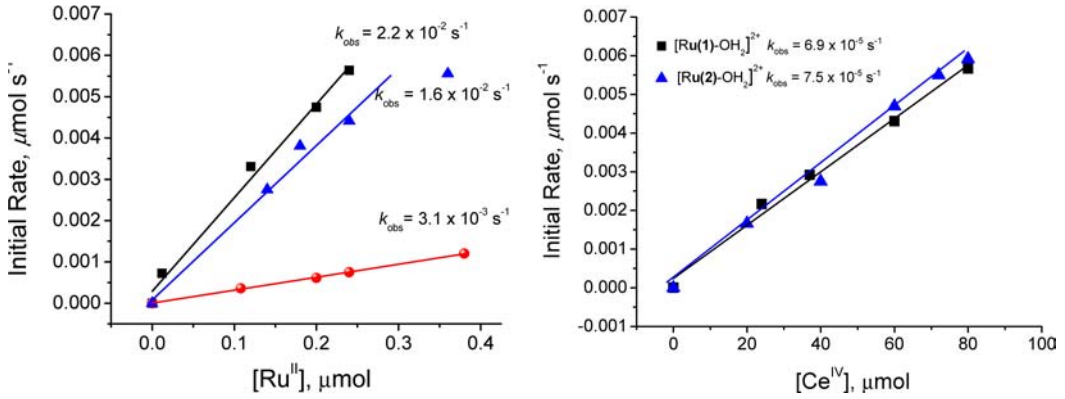

Figure 2. Plots of the initial rates for O_2 evolution with $[\mathbf{Ru(1)}{-}OH_2]^{2+}$ (black squares), $[\mathbf{Ru(2)}{-}OH_2]^{2+}$ (blue triangles), and $[Ru(tpy)(bpm)(H_2O)]^{2+}$ (red circles). Left: As a function of [Ru] in 0.1 M HNO_3 with $[Ce^{IV}]$ = 0.01 M (4×10^{-5} mol, 4 mL). For $[Ru(tpy)(bpm)(H_2O)]^{2+}$, 0.5 M HNO_3 was used. Right: As a function of $[Ce^{IV}]$ (μmol) at fixed concentration of Ru(II): $[\mathbf{Ru^{II}(1)}{-}OH_2]^{2+}$ (black, 3.2×10^{-5} M, 0.128 μmol, 4 mL) and $[\mathbf{Ru^{II}(2)}{-}OH_2]^{2+}$ (blue, 4.5×10^{-5} M, 0.18 μmol, 4 mL).

and 1.6 ± 0.1 M^{-1} s^{-1}, respectively (see the Supporting Information for more details). These kinetic data are in contrast to the zero-order dependence in $[Ce^{IV}]$ at pH 1 found for previously investigated Ru(II) polypyridines (e.g., $Ru^{II}(tpy)(bpm)(OH_2)]^{2+}$) in which the thermal evolution of O_2 from an $[Ru^{IV}{-}OO]^{2+}$ species was assigned as the rate-determining step (RDS).[18,20] Although we cannot define the exact elementary RDS, the first-order dependency in $[Ce^{IV}]$ (pH 1) for $[\mathbf{Ru^{II}(1)}{-}OH_2]^{2+}$ and $[\mathbf{Ru^{II}(2)}{-}OH_2]^{2+}$ is in agreement with our previous report[23] that the $[\mathbf{Ru^{IV}(1)}{-}OO]^{2+}$ species requires an additional equivalent of Ce(IV) oxidant to release O_2.

Moreover, the UV–vis absorption spectrum of $[\mathbf{Ru^{IV}(2)}{=}O]^{2+}$ obtained by Ce(IV) oxidation of $[\mathbf{Ru^{II}(2)}{-}OH_2]^{2+}$ (Supporting Information, Figure S7) is similar to the two-electron oxidized intermediate generated from the aqueous solutions of $[\mathbf{Ru^{II}(1)}{-}OH_2]^{2+}$ either by Ce(IV) at pH 1 or pulse radiolysis experiments with an excess of carbonate radicals (1.59 V) at pH 10.5.[23] Subsequent chemical reduction of the two-electron oxidized $[\mathbf{Ru^{IV}(2)}{=}O]^{2+}$ species with Fe(II) led to the partial recovery of $[\mathbf{Ru^{II}(2)}{-}OH_2]^{2+}$ (Supporting Information, Figure S8) indicating that $[\mathbf{Ru^{IV}(2)}{=}O]^{2+}$ is more reactive than $[\mathbf{Ru^{IV}(1)}{=}O]^{2+}$.[23] A side-product that has an absorption band around 580 nm was formed together with $[\mathbf{Ru^{II}(2)}{-}OH_2]^{2+}$. In contrast to $[Ru^{II}(tpy)(bpm)(OH_2)]^{2+}$ and $[Ru^{II}(tpy)(bpy)(OH_2)]^{2+}$, the one- and two-electron oxidized forms of $[\mathbf{Ru^{II}(2)}{-}OH_2]^{2+}$ are unstable in aqueous media (pH 1). Thus, we measured the UV–vis absorption spectra of the transient $[\mathbf{Ru^{III}(2)}{-}OH]^{2+}$ and $[\mathbf{Ru^{IV}(2)}{=}O]^{2+}$ species by pulse radiolysis at pH 10.5. The detailed procedure and results are shown in Supporting Information, Figures S9–S14. The transient spectra of $[\mathbf{Ru^{III}(2)}{-}OH]^{2+}$ and $[\mathbf{Ru^{IV}(2)}{=}O]^{2+}$ produced by pulse radiolysis are analogous to those of $[\mathbf{Ru^{III}(1)}{-}OH]^{2+}$ and $[\mathbf{Ru^{IV}(1)}{=}O]^{2+}$, respectively. The $[Ru^{III}{-}OH]^{2+}$ species disproportionates to form $[Ru^{II}{-}OH_2]^{2+}$ and $[Ru^{IV}{=}O]^{2+}$ with a rate constant on the same order of magnitude as for $[\mathbf{Ru^{III}(1)}{-}OH]^{2+}$ (k_{disp} = (6.5 ± 0.5) × 10^3 M^{-1} s^{-1} and (8.3 ± 0.5) × 10^3 M^{-1} s^{-1} for $[\mathbf{Ru^{III}(1)}{-}OH]^{2+}$[23] and $[\mathbf{Ru^{III}(2)}{-}OH]^{2+}$ respectively; Supporting Information, Figure S12).

Electrochemical Studies and Mechanistic Investigations. The pH-dependent cyclic and square-wave voltammograms of $[\mathbf{Ru^{II}(2)}{-}OH_2]^{2+}$ were measured in 10 mM Britton–Robinson buffer with a glassy carbon working electrode (Supporting Information, Figures S15 and S16). The resulting Pourbaix diagram is shown in Figure 3, and is quite similar to

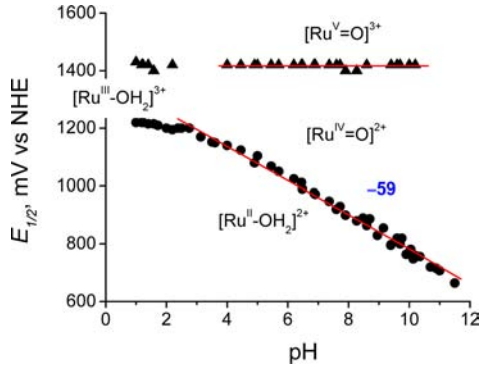

Figure 3. Pourbaix diagram of $[\mathbf{Ru^{II}(2)}{-}OH_2]^{2+}$ in 10 mM Britton–Robinson buffer, 0.1 M triflate and 20% 2,2,2-trifluoroethanol obtained from square-wave voltammograms performed by scans in a positive direction from 200 to 1600 mV.

that of $[\mathbf{Ru^{II}(1)}{-}OH_2]^{2+}$ published previously,[23] but differs notably from those of $[Ru(tpy)(NN)(OH_2)]^{2+}$ (NN = bpm, bpy). In particular, the pH-independent $[Ru^{V}{=}O]/[Ru^{IV}{=}O]$ couples at 1.42 V for $[\mathbf{Ru^{II}(1)}{-}OH_2)]^{2+23}$ and $[\mathbf{Ru(2)}{-}OH_2]^{2+}$ are lower than those of $[Ru(tpy)(NN)(OH_2)]^{2+}$ (NN = bpm, 1.65 V; NN = bpy, 1.73 V).[18,20] The DFT calculated Pourbaix diagram of $[\mathbf{Ru(2)}{-}OH_2]^{2+}$ is shown in Supporting Information, Figure S17, and supports the experimental findings of a coupled two-electron, two-proton oxidation to form $[\mathbf{Ru(2)}{=}O]^{2+}$ and an unusually low potential for the $[\mathbf{Ru(2)}{=}O]^{2+}/[\mathbf{Ru(2)}{=}O]^{3+}$ couple.

Background subtracted catalytic currents in cyclic voltammograms (CVs) of $[\mathbf{Ru(1)}{-}OH_2]^{2+}$ and $[\mathbf{Ru(2)}{-}OH_2]^{2+}$ at various pH values are shown in Figures 4a and 4b. Since a precise onset potential for O_2 evolution at each pH was difficult to determine, we employed the potential causing a 50% current increase compared to the corresponding $Ru^{IV/II}$ peak current. The pH-dependent onset potentials for water oxidation exhibit a slope of −59 mV/pH particularly in the pH range from 4 to 11, consistent with a PCET process (Figures 4d and 4e). These results support our mechanistic proposal that under neutral and basic conditions, catalytic water oxidation for both $[\mathbf{Ru(1)}{-}OH_2]^{2+}$ and $[\mathbf{Ru(2)}{-}OH_2]^{2+}$ is triggered by a $1H^+/1e^-$

dx.doi.org/10.1021/ic401023w | Inorg. Chem. 2013, 52, 8845–8850

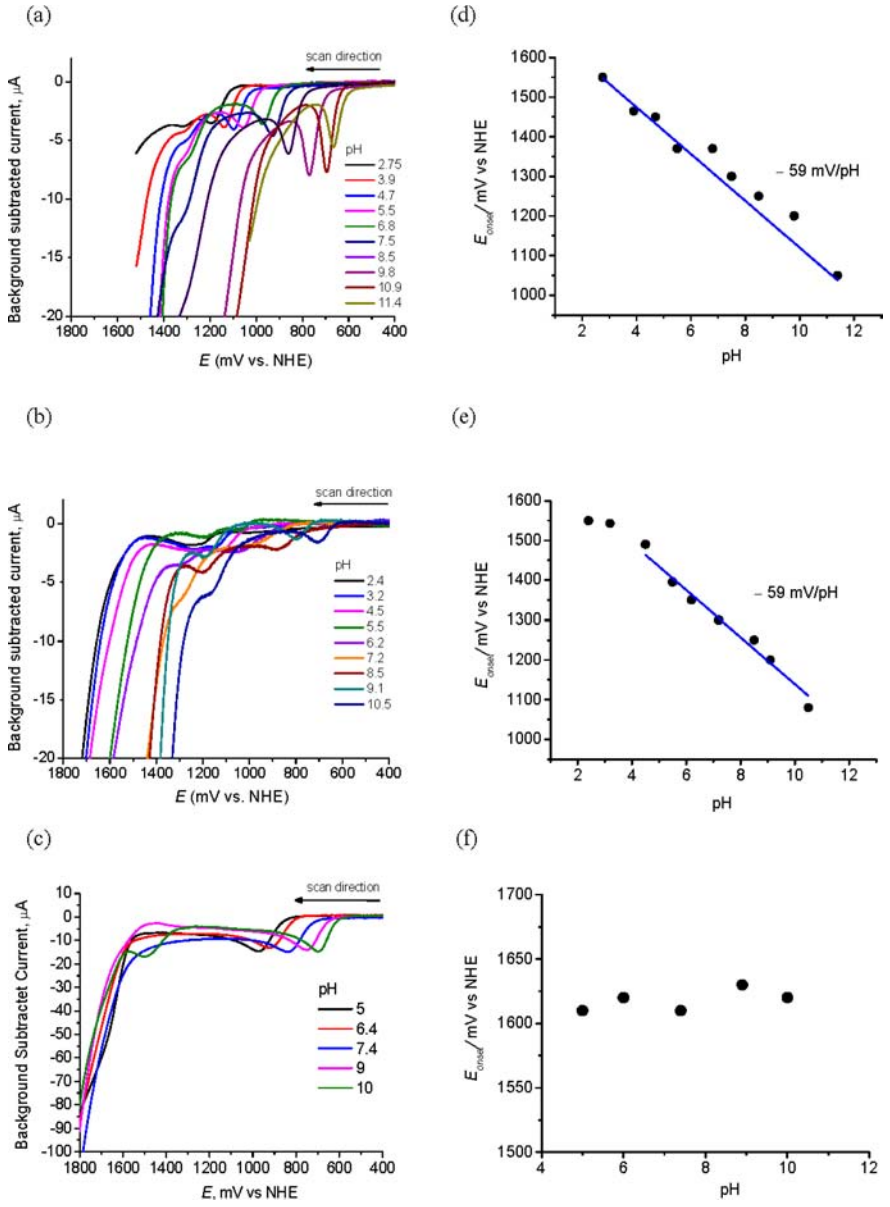

Figure 4. Panels (a), (b), and (c): Background-subtracted linear sweep voltammograms of $[\mathbf{Ru^{II}(1)}{-}OH_2]^{2+}$, $[\mathbf{Ru^{II}(2)}{-}OH_2]^{2+}$, and $[Ru^{II}(tpy)(bpm)(OH_2)]^{2+}$ complexes recorded as a function of pH. Conditions: $[\mathbf{Ru^{II}(1)}{-}OH_2]^{2+}$ was recorded in 10 mM citrate, 10 mM borate, 0.1 M triflate, and 20% 2,2,2-trifluoroethanol, and $[\mathbf{Ru^{II}(2)}{-}OH_2]^{2+}$ and $[Ru^{II}(tpy)(bpm)(OH_2)]^{2+}$ were both performed in 20 mM Britton–Robinson buffer (only half-oxidation waves are shown for clarity); scan rate: 50 mV s^{-1} (scan direction from 0.4 to 1.8 V vs NHE). Panels (d), (e), and (f): Plots of the onset oxidation potentials (E_{onset}) (determined at a 50% current increase compared to the corresponding $Ru^{IV/II}$ current) as a function of pH. In the cases of $[\mathbf{Ru^{II}(1)}{-}OH_2]^{2+}$ and $[\mathbf{Ru^{II}(2)}{-}OH_2]^{2+}$ slopes of −59 mV/pH were obtained as shown in panels (d) and (e).

pathway involving the $[Ru^{IV}{=}O]^{2+}$ species and water with concomitant removal of a proton and an electron. In fact, the onset potentials for catalytic water oxidation in the pH region of 7–11 are lower than the $Ru^{V}{=}O/Ru^{IV}{=}O$ redox couple (1.42 V), thereby exhibiting lower overpotentials in alkaline media. Under acidic conditions, however, the onset potentials remain constant at approximately 1.6 V, indicating that the "water nucleophilic attack pathway" via $[Ru^{V}{=}O]^{3+}$ plays the major role in the formation of the O–O bond.

In contrast to $[\mathbf{Ru(1)}{-}OH_2]^{2+}$ and $[\mathbf{Ru(2)}{-}OH_2]^{2+}$, the onset potentials of catalytic water oxidation mediated by $Ru^{II}(tpy)(NN)(OH_2)]^{2+}$ (NN = bpm, bpy) measured under identical experimental conditions showed negligible pH-dependency between pH 5–11 with potentials close to or higher than that of the Ru^{V}/Ru^{IV} couple (ca. 1.6–1.8 V vs NHE) (Figures 4c and 4f, and Supporting Information, Figure S18). Considering the possible slow reactivity of the $[Ru^{IV}{=}O]^{2+}$ species in $Ru^{II}(tpy)(NN)(OH_2)]^{2+}$ (NN = bpm, bpy), we carried out controlled-potential electrolysis experiments at 1.25 V (350 mV below Ru^{V}/Ru^{IV}) at pH 6 that resulted in a net $2e^{-}$ oxidation process. Spectral changes and ESI/MS data were consistent with the formation of the $[Ru^{IV}{=}O]^{2+}$ species and not the $[Ru^{IV}{-}OO]^{2+}$ species. Thus, our results clearly show that for catalysts $[Ru^{II}(tpy)(bpm)(OH_2)]^{2+}$ and $[Ru^{II}(tpy)(bpy)(OH_2)]^{2+}$, the "water nucleophilic attack" mechanism via $[Ru^{V}{=}O]^{2+}$ is operational not only at low pH as has been thoroughly investigated by Meyer[39] and Berlinguette,[20,21] but also in neutral and basic media (Scheme 1).

dx.doi.org/10.1021/ic401023w | Inorg. Chem. 2013, 52, 8845–8850

Scheme 1. Water Oxidation Mechanisms at Neutral and Basic Conditions

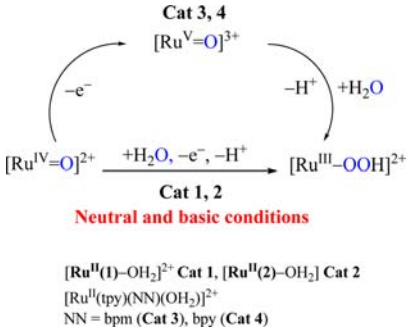

Furthermore, electrochemical oxidations of $[\mathbf{Ru(2)}{-}OH_2]^{2+}$ at a constant applied potential of 1300 mV vs NHE (120 mV below $E_{1/2}$ for the Ru^V/Ru^{IV} couple) for 10 s followed by scans performed in the cathodic direction (1300 to 200 mV) allowed us to observe the build-up of new oxidized species with pH-dependent behavior between pH 1−11 (Figure 5). Similar to

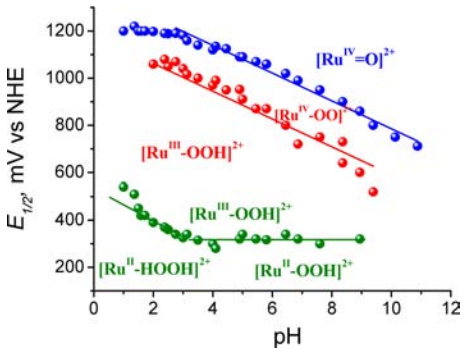

Figure 5. Pourbaix diagram of electrochemical oxidation of $[\mathbf{Ru^{II}(2)}{-}OH_2]^{2+}$(right) in 10 mM Britton−Robinson Buffer, 0.1 M triflate and 20% 2,2,2-trifluoroethanol at an applied potential of 1300 mV vs NHE; scans were performed in the cathodic direction from 1300 to 200 mV; quiet time = 10 s.

the case of the $[\mathbf{Ru(1)}{-}OH_2]^{2+}$ complex, these data for $[\mathbf{Ru(2)}{-}OH_2]^{2+}$ provide further evidence that O−O bond formation occurs by a direct PCET process between water and the $[Ru^{IV}{=}O]^{2+}$ species to yield the corresponding oxidation products $[Ru^{III}{-}OOH]^{2+}$ and subsequently $[Ru^{IV}{-}OO]^{2+}$ (red line). $[Ru^{III}{-}OOH]^{2+}$ can be further reduced to $[Ru^{II}{-}OOH]^{+}$ (and/or its protonated species at low pH, green line). A similar behavior for the $[Ru^{III}{-}OOH]^{2+}$ and $[Ru^{IV}{-}OO]^{2+}$ species was obtained in the DFT calculated Pourbaix diagram shown in Supporting Information, Figure S19. The calculated Latimer−Frost diagram showing the free energy change along the reaction path under standard conditions is shown in Supporting Information, Figure S20.

The origin of the different pathway for O−O bond formation with $[\mathbf{Ru(1)}{-}OH_2]^{2+}$ and $[\mathbf{Ru(2)}{-}OH_2]^{2+}$ complexes is not clear. These catalysts have N-bases in the second coordination sphere, and the X-ray structures show that the coordinated water molecule makes a hydrogen bond to one of the N-bases in both structures. Both catalysts show coupled $2e^-/2H^+$ oxidation to form $[Ru^{IV}{=}O]^{2+}$, which can be further oxidized to $[Ru^{V}{=}O]^{3+}$ at relatively low potential (1.42 V vs NHE) contrast to the behavior of $[Ru(tpy)(NN)(OH_2)]^{2+}$ (NN = bpy, bpm). It could perhaps be related to the coordinated water being an equatorial ligand in the present class of complexes, but an axial ligand in the $[Ru(tpy)(NN)(OH_2)]^{2+}$ complexes. To examine the role that pendent bases play in the oxidation chemistry of ruthenium polypyridyl complexes, we have previously isolated the compounds *p*-$[Ru(tpy)(pynap)(OH_2)]^{2+}$ (*p* = proximal, pynap = 2-(pyrid-2′-yl)-1,8-naphthyridine) and *d*-$[Ru(tpy)(pynap)(OH_2)]^{2+}$ (*d* = distal).[26] The X-ray structure of *p*-$[Ru(tpy)(pynap)(OH_2)]^{2+}$ shows a hydrogen-bonding interaction between the uncoordinated naphthyridyl nitrogen and the aqua ligand. While this complex exhibits coupled $2e^-/2H^+$ oxidation to form $[Ru^{IV}{=}O]^{2+}$ (pH > 4) and has a low oxidation potential to form $[Ru^{V}{=}O]^{3+}$, hardly any catalytic activity for water oxidation by Ce(IV) was observed.[26,45] The low catalytic activity of *p*-$[Ru(tpy)(pynap)(OH_2)]^{2+}$ might be due to decomposition of the complex by the use of the strong Ce(IV) oxidant as CO_2 was detected together with O_2 after the oxidation. Interestingly *d*-$[Ru(tpy)(pynap)(OH_2)]^{2+}$ is an excellent WOC showing 3200 TON with the initial rate 1.8×10^{-2} s^{-1} for O_2 evolution ($E_{1/2}$ for the $Ru^{V}{=}O/Ru^{IV}{=}O$ couple ∼1.40 V vs NHE). While photoisomerization of *d*-$[Ru(tpy)(pynap)(OH_2)]^{2+}$ to *p*-$[Ru(tpy)(pynap)(OH_2)]^{2+}$ takes place easily under ambient light, the detailed characterization of intermediates in water oxidation catalyzed by *d*-$[Ru(tpy)(pynap)(OH_2)]^{2+}$ at various pH might provide some clue.

CONCLUSIONS

We have demonstrated that the family of WOCs $[\mathbf{Ru(1)}{-}OH_2]^{2+}$ and $[\mathbf{Ru(2)}{-}OH_2]^{2+}$ show unique mechanistic behavior during the O−O bond formation step. In contrast to other mononuclear Ru polypyridyl catalysts which require high energy $[Ru^{V}{=}O]^{3+}$ intermediates to produce the corresponding hydroperoxo species, the O−O bond formation with $[\mathbf{Ru(1)}{-}OH_2]^{2+}$ and $[\mathbf{Ru(2)}{-}OH_2]^{2+}$ complexes can proceed by the thermodynamically more favorable "direct pathway" via $[Ru^{IV}{=}O]^{2+}$, which avoids the higher oxidation state $[Ru^{V}{=}O]^{3+}$ complex in neutral and basic media. Our evidence for this unique and common mechanism was provided mainly by the following: (1) pH-dependent onset catalytic potentials indicative of PCET driven catalysis; and (2) observation of electrochemical oxidation products due to O−O bond formation (e.g., $[\mathbf{Ru^{IV}}{-}OO]^{2+}$ and $[\mathbf{Ru^{III}}{-}OOH]^{2+}$) at an applied potential below 1.42 V for the $Ru^{V}{=}O/Ru^{IV}{=}O$ couple. Analogous studies, particularly those performed under high pH conditions with ruthenium(II) polypyridines such as $[Ru(tpy)(bpm)(OH_2)]^{2+}$ and $[Ru(tpy)(bpy)(OH_2)]^{2+}$ reveal the apparent classic requirement for the formation of $[Ru^{V}{=}O]^{3+}$ to initiate catalytic water-oxidation. Unlike other $[Ru(tpy)(NN)(H2O)]^{2+}$ complexes (where NN represents 2,2′-bipyridine and its derivatives), the diverse water-oxidation reactivity for $[\mathbf{Ru(1)}{-}OH_2]^{2+}$ and $[\mathbf{Ru(2)}{-}OH_2]^{2+}$ is possibly attributed to the unique ligand environment which accommodates a water ligand in the equatorial binding site of the tridentate ligand. $[\mathbf{Ru^{II}(1)}{-}OH_2]^{2+}$ and $[\mathbf{Ru^{II}(2)}{-}OH_2]^{2+}$ complexes both provide a functional model for the design of an efficient artificially photosynthetic device that proceeds by four consecutive PCET steps.

ASSOCIATED CONTENT

Supporting Information

Crystallographic data in CIF format. Further details are given in Figures S1−S20 and Tables S1−S6. This material is available free of charge via the Internet at http://pubs.acs.org.

dx.doi.org/10.1021/ic401023w | Inorg. Chem. 2013, 52, 8845−8850

AUTHOR INFORMATION

Corresponding Author

*E-mail: dmitriyp@bnl.gov (D.P.), fujita@bnl.gov (E.F.).

Notes

The authors declare no competing financial interest.

ACKNOWLEDGMENTS

We thank Natawutt Kaveevivitchai for TON measurements by Method 1. The work at Brookhaven National Laboratory (BNL) is funded under contract DE-AC02-98CH10886 and the work at Houston is funded under contract DE-FG02-07ER15888 with the U.S. Department of Energy and supported by its Division of Chemical Sciences, Geosciences, & Biosciences, Office of Basic Energy Sciences. The BNL authors also thank the U.S. Department of Energy for funding under the BES Hydrogen Fuel Initiative. R.H., R.Z., and R.P.T. also thank the Robert A. Welch Foundation (E-621).

REFERENCES

(1) Lewis, N. S.; Nocera, D. G. *Proc. Natl. Acad. Sci. U.S.A.* **2007**, *104*, 20142−20142.
(2) Kanan, M. W.; Nocera, D. G. *Science* **2008**, *321*, 1072−1075.
(3) Pace, R. J. In *Artificial Photosynthesis*; Critchley, A. C. a. C., Ed.; Wiley-VCH: Weinheim, Germany, 2005, Chapter 2.
(4) Concepcion, J. J.; Jurss, J. W.; Brennaman, M. K.; Hoertz, P. G.; Patrocinio, A. O. T.; Iha, N. Y. M.; Templeton, J. L.; Meyer, T. J. *Acc. Chem. Res.* **2009**, *42*, 1954−1965.
(5) Liu, X.; Wang, F. Y. *Coord. Chem. Rev.* **2012**, *256*, 1115−1136.
(6) Hetterscheid, D. G. H.; Reek, J. N. H. *Angew. Chem., Int. Ed.* **2012**, *51*, 9740−9747.
(7) Cao, R.; Lai, W. Z.; Du, P. W. *Energy Environ. Sci.* **2012**, *5*, 8134−8157.
(8) Wasylenko, D. J.; Palmer, R. D.; Berlinguette, C. P. *Chem. Commun.* **2013**, *49*, 218−227.
(9) McEvoy, J. P.; Brudvig, G. W. *Chem. Rev.* **2006**, *106*, 4455−4483.
(10) Meyer, T. J.; Huynh, M. H. V.; Thorp, H. H. *Angew. Chem., Int. Ed.* **2007**, *46*, 5284−5304.
(11) Huynh, M. H. V.; Meyer, T. J. *Chem. Rev.* **2007**, *107*, 5004−5064.
(12) Umena, Y.; Kawakami, K.; Shen, J.-R.; Kamiya, N. *Nature* **2011**, *473*, 55−60.
(13) Weinberg, D. R.; Gagliardi, C. J.; Hull, J. F.; Murphy, C. F.; Kent, C. A.; Westlake, B. C.; Paul, A.; Ess, D. H.; McCafferty, D. G.; Meyer, T. J. *Chem. Rev.* **2012**, *112*, 4016−4093.
(14) Gagliardi, C. J.; Vannucci, A. K.; Concepcion, J. J.; Chen, Z. F.; Meyer, T. J. *Energy Environ. Sci.* **2012**, *5*, 7704−7717.
(15) Gersten, S. W.; Samuels, G. J.; Meyer, T. J. *J. Am. Chem. Soc.* **1982**, *104*, 4029−4030.
(16) Zong, R.; Thummel, R. P. *J. Am. Chem. Soc.* **2005**, *127*, 12802−12803.
(17) Tseng, H. W.; Zong, R.; Muckerman, J. T.; Thummel, R. *Inorg. Chem.* **2008**, *47*, 11763−11773.
(18) Concepcion, J. J.; Jurss, J. W.; Templeton, J. L.; Meyer, T. J. *J. Am. Chem. Soc.* **2008**, *130*, 16462.
(19) Masaoka, S.; Sakai, K. *Chem. Lett.* **2009**, *38*, 182−183.
(20) Wasylenko, D. J.; Ganesamoorthy, C.; Koivisto, B. D.; Henderson, M. A.; Berlinguette, C. P. *Inorg. Chem.* **2010**, *49*, 2202−2209.
(21) Wasylenko, D. J.; Ganesamoorthy, C.; Henderson, M. A.; Koivisto, B. D.; Osthoff, H. D.; Berlinguette, C. P. *J. Am. Chem. Soc.* **2010**, *132*, 16094−16106.
(22) Yagi, M.; Tajima, S.; Komi, M.; Yamazaki, H. *Dalton Trans.* **2011**, *40*, 3802−3804.
(23) Polyansky, D. E.; Muckerman, J. T.; Rochford, J.; Zong, R. F.; Thummel, R. P.; Fujita, E. *J. Am. Chem. Soc.* **2011**, *133*, 14649−14665.
(24) Duan, L. L.; Xu, Y. H.; Tong, L. P.; Sun, L. C. *ChemSusChem* **2011**, *4*, 238−244.
(25) Duan, L. L.; Tong, L. P.; Xu, Y. H.; Sun, L. C. *Energy Environ. Sci.* **2011**, *4*, 3296−3313.
(26) Boyer, J. L.; Polyansky, D. E.; Szalda, D. J.; Zong, R. F.; Thummel, R. P.; Fujita, E. *Angew. Chem., Int. Ed.* **2011**, *50*, 12600−12604.
(27) Kaveevivitchai, N.; Chitta, R.; Zong, R. F.; El Ojaimi, M.; Thummel, R. P. *J. Am. Chem. Soc.* **2012**, *134*, 10721−10724.
(28) Kimoto, A.; Yamauchi, K.; Yoshida, M.; Masaoka, S.; Sakai, K. *Chem. Commun.* **2012**, *48*, 239−241.
(29) Duan, L.; Bozoglian, F.; Mandal, S.; Stewart, B.; Privalov, T.; Llobet, A.; Sun, L. *Nat. Chem.* **2012**, *4*, 418−423.
(30) Wang, L.; Duan, L. L.; Stewart, B.; Pu, M. P.; Liu, J. H.; Privalov, T.; Sun, L. C. *J. Am. Chem. Soc.* **2012**, *134*, 18868−18880.
(31) Tong, L. P.; Wang, Y.; Duan, L. L.; Xu, Y. H.; Cheng, X.; Fischer, A.; Ahlquist, M. S. G.; Sun, L. C. *Inorg. Chem.* **2012**, *51*, 3388−3398.
(32) Kaveevivitchai, N.; Zong, R.; Tseng, H.-W.; Chitta, R.; Thummel, R. P. *Inorg. Chem.* **2012**, *51*, 2930−2939.
(33) Karkas, M. D.; Akermark, T.; Johnston, E. V.; Karim, S. R.; Laine, T. M.; Lee, B. L.; Akermark, T.; Privalov, T.; Akermark, B. *Angew. Chem., Int. Ed.* **2012**, *51*, 11589−11593.
(34) Vannucci, A. K.; Hull, J. F.; Chen, Z.; Binstead, R. A.; Concepcion, J. J.; Meyer, T. J. *J. Am. Chem. Soc.* **2012**, *134*, 3972−3975.
(35) Tong, L. P.; Gothelid, M.; Sun, L. C. *Chem. Commun.* **2012**, *48*, 10025−10027.
(36) Chen, Z. F.; Vannucci, A. K.; Concepcion, J. J.; Jurss, J. W.; Meyer, T. J. *Proc. Natl. Acad. Sci. U. S. A.* **2011**, *108*, 1461−1469.
(37) Chen, Z. F.; Concepcion, J. J.; Luo, H. L.; Hull, J. F.; Paul, A.; Meyer, T. J. *J. Am. Chem. Soc.* **2010**, *132*, 17670−17673.
(38) Chen, Z. F.; Concepcion, J. J.; Hull, J. F.; Hoertz, P. G.; Meyer, T. J. *Dalton Trans.* **2010**, *39*, 6950−6952.
(39) Chen, Z.; Concepcion, J. J.; Jurss, J. W.; Meyer, T. J. *J. Am. Chem. Soc.* **2009**, *131*, 15580−15581.
(40) Parent, A. R.; Crabtree, R. H.; Brudvig, G. W. *Chem. Soc. Rev.* **2012**, *42*, 2247−2252.
(41) Duan, L. L.; Araujo, C. M.; Ahlquist, M. S. G.; Sun, L. C. *Proc. Natl. Acad. Sci. U. S. A.* **2012**, *109*, 15584−15588.
(42) Concepcion, J. J.; Tsai, M. K.; Muckerman, J. T.; Meyer, T. J. *J. Am. Chem. Soc.* **2010**, *132*, 1545−1557.
(43) Chen, Z. F.; Concepcion, J. J.; Hu, X. Q.; Yang, W. T.; Hoertz, P. G.; Meyer, T. J. *Proc. Natl. Acad. Sci. U.S.A.* **2010**, *107*, 7225−7229.
(44) Romain, S.; Vigara, L.; Llobet, A. *Acc. Chem. Res.* **2009**, *42*, 1944−1953.
(45) Yamazaki, H.; Hakamata, T.; Komi, M.; Yagi, M. *J. Am. Chem. Soc.* **2011**, *133*, 8846−8849.